Inverse Problems in Engineering: Theory and Practice
3rd Int. Conference on Inverse Problems in Engineering
June 13-18, 1999, Port Ludlow, WA, USA
ID05

DETERMINATION OF MECHANICAL PROPERTIES OF THIN FILMS AND FUNCTIONAL GRADIENT MATERIALS USING INVERSE TECHNIQUE

Hideo KOGUCHI
Department of Mechanical Engineering, Nagaoka University of Technology
1603-1 Kamitomioka, Nagaoka, 940-2188 Japan
koguchi@mech.nagaokaut.ac.jp

Keywords : Inverse Problem, Contact Problem, Elasticity, Complex Method, Layered Materials, FGM

ABSTRACT

This paper describes a method for evaluating material properties of multi-layered systems and functional gradient materials using data obtained from indentation testing. The measurement data collected from the penetration force-depth curves in the test are employed for identifying elastic moduli of thin films and functional gradient materials. An indentation problem is first analyzed on the basis of the three-dimensional axisymmetric theory of elasticity. Analyses of elastic contact problem, which an elastic axisymmetric indenter is penetrated into multi-layered systems and into functional gradient materials, are presented. An inverse analysis for determining Young's moduli, Poisson's ratios and radii of the contact area is performed under the assumption that the elastic moduli of the substrate and the indenter, and thicknesses for layers are known. When complex method is used for minimizing an objective function composed of errors, effective sampling of data obtained by penetrating indenters with various radii of curvature into the coated substrate and functional gradient materials is presented.

INTRODUCTION

Modern electric devices and mass storage devices have frequently multilayered structures to achieve a high performance and functionality. Furthermore, such devices are coated often by metal thin films to protect from the damage of external dusts and environment. It is important to estimate their mechanical properties for improving the reliability of devices and machines. Generally, mechanical properties of thin films deposited on a substrate are different from those of bulk. Hence, we need to know in-situ the mechanical properties of deposited films. However, it is very hard to carry out a test for evaluating the mechanical properties of films in a sub-micrometer thickness. Ihara, et al. estimated the material properties of a thin film using surface wave spectroscopy. Matui, et al. examined the accuracy of identified elastic moduli in a multilayered system. Kishimoto, et al. idetified the elastic properties for a bar of functional gradient materials. Indentation test is one of methods for evaluating the mechanical properties of thin films, which is the one estimating elastic moduli of thin films using experimental data of the force and the depth of an indenter penetrated into a multi-layered system. In the present paper, when data of the indentation force and depth are used, a method for identifying the mechanical properties of thin films and the distribution function of mechanical properties in functional gradient materials will be presented.

ANALYSIS OF INDENTATION PROBLEMS

In the present analysis, an axisymmetric elastic indenter with a cross section of $f(r)$ will be penetrated into an elastic half-region composed of layers with various mechanical properties as shown in Figure 1. This contact problem is analyzed using the theory of three-dimensional axisymmetric elasticity. Then, displacements and stresses in the layers, the indenter and the elastic half-region can be deduced by substituting Boussinesq's potential functions, ψ and ϕ_3, into the following relationships (Miyamoto 1977, Gladwell 1980).

$$u_1^{(i)} = -\frac{1}{2\mu_i}\left\{\frac{\partial \psi^{(i)}}{\partial r} + z\frac{\partial \phi_3^{(i)}}{\partial r}\right\} \tag{1}$$

$$u_3^{(i)} = \frac{1}{2\mu_i}\left\{\kappa_i \phi_3^{(i)} - z\frac{\partial \phi_3^{(i)}}{\partial z} - \frac{\partial \psi^{(i)}}{\partial z}\right\} \tag{2}$$

$$\sigma_{11}^{(i)} = \frac{1}{r}\frac{\partial \psi^{(i)}}{\partial r} + \frac{\partial^2 \psi^{(i)}}{\partial z^2} + \frac{z}{r}\frac{\partial \phi_3^{(i)}}{\partial r} + z\frac{\partial^2 \phi_3^{(i)}}{\partial r^2} + 2\nu_i \frac{\partial \phi_3^{(i)}}{\partial z} \tag{3}$$

$$\sigma_{22}^{(i)} = -\frac{1}{r}\frac{\partial \psi^{(i)}}{\partial r} - \frac{z}{r}\frac{\partial \phi_3^{(i)}}{\partial r} + 2\nu_i \frac{\partial \phi_3^{(i)}}{\partial z} \tag{4}$$

$$\sigma_{33}^{(i)} = -\frac{\partial^2 \psi^{(i)}}{\partial z^2} - z\frac{\partial^2 \phi_3^{(i)}}{\partial z^2} + \frac{1+\kappa_i}{2}\frac{\partial \phi_3^{(i)}}{\partial z} \tag{5}$$

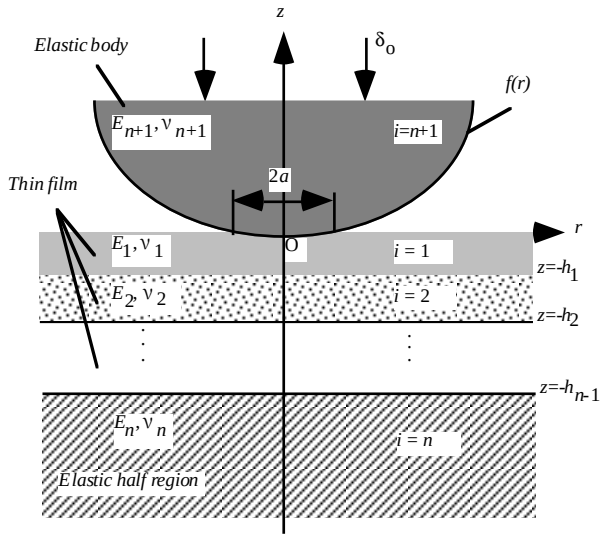

Figure 1 Model for Analysis and Coordinate System

$$\sigma_{13}^{(i)} = -\frac{\partial}{\partial r}\left\{\frac{\partial \psi^{(i)}}{\partial z} + z\frac{\partial \phi_3^{(i)}}{\partial z} + \frac{1-\kappa_i}{2}\phi_3^{(i)}\right\} \tag{6}$$

where the upper suffix i indicates the number of film, κ_i=3-4 ν_i, ν_i represents Poisson's ratio of the films and the indenter.

In this analysis, the thickness of film is constant and uniform, and every film adheres perfectly to each other. Then, the boundary condition for analysis can be expressed as follows;

(I) At the i th interface (z=-h_i : i=1,…, n-1)

$$u_1^{(i)} = u_1^{(i+1)},\ u_3^{(i)} = u_3^{(i+1)} \tag{7}$$

$$\sigma_{33}^{(i)} = \sigma_{33}^{(i+1)},\ \sigma_{13}^{(i)} = \sigma_{13}^{(i+1)} \tag{8}$$

(II) At the top surface of film (z=0)

$$\sigma_{13}^{(1)} = 0 \tag{9}$$

$$\sigma_{33}^{(1)}(r,0) - p(r) = 0,\ p(r,0) = 0\ \ (r \geq a) \tag{10}$$

(III) At the surface of the indenter (z=0)

$$\sigma_{13}^{(n+1)} = 0 \tag{11}$$

$$-\sigma_{33}^{(n+1)}(r,0) + p(r) = 0 \tag{12}$$

(IV) At the contact area ($0 \leq r \leq a$, z=0)

$$-u_3^{(1)}(r,0) + u_3^{(n+1)}(r,0) = \delta_0 - f(r) \tag{13}$$

where δ_0 represents the penetrated depth of the indenter, and $f(r)$ represents the cross section of the indenter.

(V) At an infinity ($r \to \infty$, $z \to \pm\infty$)

All components of displacement and stress vanish.

Where a represents the radius of contact area, and $p(r)$ represents the distribution of contact pressure.

Considering the boundary condition (V), the following Boussinesq's potential functions, ϕ_3 and ψ are used.

Potential functions for films (i=1,…,n-1)

$$\phi_3^{(i)} = \int_0^\infty J_0(\lambda r)\left\{C_1^i(\lambda)e^{\lambda z} + C_2^i(\lambda)e^{-\lambda z}\right\}d\lambda \tag{14}$$

$$\psi^{(i)} = \int_0^\infty J_0(\lambda r)\left\{C_3^i(\lambda)e^{\lambda z} + C_4^i(\lambda)e^{-\lambda z}\right\}d\lambda \tag{15}$$

Potential functions for an elastic half-space (i=n)

$$\phi_3^{(n)} = \int_0^\infty J_0(\lambda r)C_1^n(\lambda)e^{\lambda z}d\lambda \tag{16}$$

$$\psi^{(n)} = \int_0^\infty J_0(\lambda r)C_3^n(\lambda)e^{\lambda z}d\lambda \tag{17}$$

Potential functions for the indenter (i=n+1)

$$\phi_3^{(n+1)} = \int_0^\infty J_0(\lambda r)C_2^{n+1}(\lambda)e^{-\lambda z}d\lambda \tag{18}$$

$$\psi^{(n+1)} = \int_0^\infty J_0(\lambda r)C_4^{n+1}(\lambda)e^{-\lambda z}d\lambda \tag{19}$$

where $J_0(x)$ represents the 0th order of the first kind Bessel function, and several unknown functions, $C_1^j(\lambda),\cdots,C_4^j(\lambda)$, included in the potential functions should be determined from the boundary conditions.

Determination of The Unknown Functions

Here, dimensionless variables divided with the thickness of the first film, h_1, or transverse elastic modulus of the first film, μ_1, are introduced in the analysis. Substituting the stresses and displacements into the relationships of the boundary condition (I) and equating integrands in each relationship yields the following matrix expression for the unknown functions.

$$\boldsymbol{R}_i\overline{\boldsymbol{C}}^i = \boldsymbol{R}_{i+1}\overline{\boldsymbol{C}}^{i+1}\ \text{(i=1,..., n-1)}, \tag{20}$$

where

$$\overline{\boldsymbol{C}}^i = \begin{bmatrix}\overline{C}_1^i & \overline{C}_2^i & \overline{\overline{C}}_3^i & \overline{\overline{C}}_4^i\end{bmatrix}^T. \tag{21}$$

Where $\boldsymbol{R}_i$ represents a coefficient matrix derived from the potential function of the ith layer and is shown as

$$\boldsymbol{R}_i = \begin{bmatrix} \frac{\bar{\lambda}\bar{h}_i}{\Gamma_i}e^{-\bar{\lambda}\bar{h}_i} & \frac{\bar{\lambda}\bar{h}_i}{\Gamma_i}e^{\bar{\lambda}\bar{h}_i} & -\frac{1}{\Gamma_i}e^{-\bar{\lambda}\bar{h}_i} & -\frac{1}{\Gamma_i}e^{\bar{\lambda}\bar{h}_i} \\ \frac{\kappa_i + \bar{\lambda}\bar{h}_i}{\Gamma_i}e^{-\bar{\lambda}\bar{h}_i} & \frac{\kappa_i - \bar{\lambda}\bar{h}_i}{\Gamma_i}e^{\bar{\lambda}\bar{h}_i} & -\frac{1}{\Gamma_i}e^{-\bar{\lambda}\bar{h}_i} & \frac{1}{\Gamma_i}e^{\bar{\lambda}\bar{h}_i} \\ \left(K_i + \bar{\lambda}\bar{h}_i\right)e^{-\bar{\lambda}\bar{h}_i} & \left(-K_i + \bar{\lambda}\bar{h}_i\right)e^{\bar{\lambda}\bar{h}_i} & -e^{-\bar{\lambda}\bar{h}_i} & -e^{\bar{\lambda}\bar{h}_i} \\ \left(\Lambda_i + \bar{\lambda}\bar{h}_i\right)e^{-\bar{\lambda}\bar{h}_i} & \left(\Lambda_i - \bar{\lambda}\bar{h}_i\right)e^{\bar{\lambda}\bar{h}_i} & -e^{-\bar{\lambda}\bar{h}_i} & e^{\bar{\lambda}\bar{h}_i} \end{bmatrix}, \tag{22}$$

where

$$K_i = (1+\kappa_i)/2,\ \Lambda_i = (-1+\kappa_i)/2,\ \bar{h}_i = h_i/h_1,\ \bar{\lambda} = \lambda h,\ \Gamma_i = \mu_i/\mu_1$$

$$\overline{C}_j^i = C_j^i h\ \ (j=1,\cdots,4),\ \overline{\overline{C}}_3^i = \bar{\lambda}\overline{C}_3^i/h_1,\ \overline{\overline{C}}_4^i = \bar{\lambda}\overline{C}_4^i/h_1. \tag{23}$$

Using the relationship of eq.(20), the ith unknown function in a vector form $\overline{\boldsymbol{C}}^i$ can be expressed by the nth unknown function $\overline{\boldsymbol{C}}^n$, which represents the function for the elastic half-region.

$$\overline{\boldsymbol{C}}^i = \prod_{j=i}^{n-1}\left[\boldsymbol{R}_j^{-1}\cdot\boldsymbol{R}_{j+1}\right]\overline{\boldsymbol{C}}^n = {}^*\boldsymbol{R}^{(i)}\cdot\overline{\boldsymbol{C}}^n \tag{24}$$

Relationships of $\overline{C}_1^n$, $\overline{\overline{C}}_3^n$, $\overline{C}_2^{n+1}$ and $\overline{\overline{C}}_4^{n+1}$ are deduced using the boundary conditions (II) and (III).

From the boundary condition (II)

$$-\Lambda_1\left(\overline{C}_1^1 + \overline{C}_2^1\right) + \overline{\overline{C}}_3^1 - \overline{\overline{C}}_4^1 = 0 \tag{25}$$

$$\int_0^\infty \bar{\lambda}J_0(\bar{\lambda}\bar{r})\left\{K_1\overline{C}_1^1 - K_1\overline{C}_2^1 - \overline{\overline{C}}_3^1 - \overline{\overline{C}}_4^1\right\}d\bar{\lambda} - p(r)h_1^3 = 0 \tag{26}$$

From the boundary condition (III)

$$-\Lambda_{n+1}\overline{C}_2^{n+1} - \overline{\overline{C}}_4^{n+1} = 0 \tag{27}$$

$$\int_0^\infty \bar{\lambda}J_0(\bar{\lambda}\bar{r})\left\{K_{n+1}\overline{C}_2^{n+1} + \overline{\overline{C}}_4^{n+1}\right\}d\bar{\lambda} + p(r)h_1^3 = 0 \tag{28}$$

Using eqs.(25)-(27), the unknown functions, $\overline{C}_1^n$, $\overline{\overline{C}}_3^n$ and $\overline{\overline{C}}_4^{n+1}$ are represented by $\overline{\overline{C}}_2^{n+1}$.

$$\overline{C}_1^n = -\frac{f_2}{\Delta}\overline{C}_2^{n+1},\ \overline{\overline{C}}_3^n = \frac{f_1}{\Delta}\overline{C}_2^{n+1},\ \overline{\overline{C}}_4^{n+1} = -\Lambda_{n+1}\overline{C}_2^{n+1} \tag{29}$$

where $\Delta = f_2 f_3 - f_1 f_4$.

Substituting eq.(29) into eq.(28) yields

$$\int_0^\infty \bar{\lambda}J_0(\bar{\lambda}\bar{r})\overline{C}_2^{n+1}d\bar{\lambda} + p(r)h_1^3 = 0. \tag{30}$$

When the Hankel inverse transformation is applied to eq.(30), the unknown function $\overline{C}_2^{n+1}$ can be expressed by the function of contact pressure. Hence, all the unknown functions are expressed using the contact pressure, which is the unknown function of r.

Integral Equation for The Contact Pressure

The contact pressure can be determined by solving an integral equation deduced from the boundary condition (IV) as follows.

$$\int_0^\infty\left\{\frac{f_1 f_5}{\Delta} + \frac{K_{n+1}}{\Gamma_{n+1}}\right\}J_0(\bar{\lambda}\bar{r})\int_0^{\bar{a}}\bar{r}'J_0(\bar{\lambda}\bar{r}')\bar{p}(\bar{r}')d\bar{r}'\,d\bar{\lambda} = 2\left\{\bar{f}(\bar{r}) - \bar{\delta}_0\right\} \tag{31}$$

where

$$\bar{\delta}_0 = \frac{\delta_0}{h_1},\ \ \bar{f}(\bar{r}) = \frac{f(\bar{r})}{h_1} \tag{32}$$

The distribution of contact pressure is expressed using a series expansion of the 2kth order of the first kind Legendre function to solve the integral equation (31).

$$\bar{p}(\bar{r}') = \frac{1}{\bar{a}\sqrt{1-(\bar{r}'/\bar{a})^2}} \sum_{k=0}^{\infty} \bar{p}_k \frac{P_{2k}\left(\sqrt{1-(\bar{r}'/\bar{a})^2}\right)}{P_{2k}(0)} \tag{33}$$

Substituting eq.(33) into eq.(31), integrating the equation from 0 to $\bar{a}$, then multiplying

$$\frac{\bar{r}}{\bar{a}\sqrt{1-(\bar{r}/\bar{a})^2}} \frac{P_{2m}\left(\sqrt{1-(\bar{r}/\bar{a})^2}\right)}{P_{2m}(0)} \tag{34}$$

with the equation, and integrating the equation with respect to *r* yields the following simultaneous equation.

$$\bar{a}\sum_{m=0}^{\infty}\sum_{k=0}^{\infty}(-1)^{k+m}\bar{p}_k \int_0^{\infty}\left\{\frac{f_1 f_5}{\Delta}+\frac{K_{n+1}}{\Gamma_{n+1}}\right\} j_{2k}(\bar{\lambda}\bar{a}) j_{2m}(\bar{\lambda}\bar{a}) d\bar{\lambda} + 2\bar{\delta}_0\delta_{m0}$$
$$= 2\int_0^1 \bar{f}\left(\bar{a}\sqrt{1-t^2}\right)\frac{P_{2m}(t)}{P_{2m}(0)}dt, \tag{35}$$

where j_{2n} represents the 2*n*th order of the first spherical Bessel function,

$$\delta_{mn} = \begin{cases} 1 & (m=n) \\ 0 & (m\neq n) \end{cases}, \tag{36}$$

and the paraboloidal indenter with a tip of radius of curvature, R_L, can be expressed as

$$\bar{f}(\bar{r}) = \bar{r}^2 \big/ 2R_L . \tag{37}$$

Functions, f_j (*j*=1,…, 5), involved in the kernel function of eq.(35) are expressed as

$$f_1 = \Lambda_1\left({}^*R_{11}^{(1)} + {}^*R_{21}^{(1)}\right) - {}^*R_{31}^{(1)} + {}^*R_{41}^{(1)}, \tag{38}$$

$$f_2 = \Lambda_1\left({}^*R_{12}^{(1)} + {}^*R_{22}^{(1)}\right) - {}^*R_{32}^{(1)} + {}^*R_{42}^{(1)}, \tag{39}$$

$$f_3 = {}^*R_{11}^{(1)} - \kappa_1\, {}^*R_{21}^{(1)} - 2\,{}^*R_{41}^{(1)}, \tag{40}$$

$$f_4 = {}^*R_{12}^{(1)} - \kappa_1\, {}^*R_{22}^{(1)} - 2\,{}^*R_{42}^{(1)}, \tag{41}$$

$$f_5 = \left\{\kappa_1\left({}^*R_{11}^{(1)} + {}^*R_{21}^{(1)}\right) - {}^*R_{31}^{(1)} + {}^*R_{41}^{(1)}\right\}\frac{f_2}{f_1} - \left\{\kappa_1\left({}^*R_{12}^{(1)} + {}^*R_{22}^{(1)}\right) - {}^*R_{32}^{(1)} + {}^*R_{42}^{(1)}\right\} \tag{42}$$

where $R_{lm}^{(i)}$ represents the component at the *l*th row and the *m*th column in the matrix ${}^*\boldsymbol{R}^{(i)}$ defined by eq.(24).

The contact pressure is determined by solving the simultaneous equation (35) with respect to $\bar{p}_k$. Then, the force for penetrating the indenter until the depth δ_0 can be expressed as follows.

$$\bar{F} = 2\pi\bar{a}\bar{p}_0 \tag{43}$$

where $\bar{p}_0$ is the first coefficient in the series expansion of contact pressure.

IDENTIFICATION OF ELASTIC MODULI OF FILMS

A method for identifying elastic moduli of each layer in a multilayered system is described in this chapter. Data on the curve of force-depth and the complex method in nonlinear optimization methods (Jacoby, et al. 1972) are used in the analysis. There are several investigations of identifying elastic moduli of thin film coated to an elastic half-region. In the field of civil engineering, pavement is regarded as an elastic region with multi-layered structures, and Novotny (1992) presented a method which determines elastic moduli for each layer from the deflection of ground by applying a piecewise uniform load to the pavement. In their investigation, the displacements and the stresses in the layers can be expressed analytically, so the sensitivity matrix for the unknown parameters can be calculated analytically. On the contrary, the sensitivity matrix is hardly derived analytically in this study, since a relationship between the penetration force and the penetration depth of the indenter is deduced by only solving the integral equation. Hence, the complex method, which is not required for the derivatives of an objective function, is used in this investigation.

The contact problem is analyzed under the assumption that the penetration force is applied within an elastic limit of materials. Furthermore, the thickness of films, the elastic moduli of the indeter and of the substrate are known, and the radii of contact area and the elastic moduli of films are unknown. The profile of indenter is paraboloidal, and the friction between the indenter and the film is neglected.

Objective Function

An example of the curve of the penetration force and the penetration depth used in an inverse analysis is shown in Figure 2. This figure represents the curve for the indenter with the radius of curvature of $10h_1$, where h_1 represents the thickness of the first layer. In this study, several pairs of curves for the indenters with various radii of curvature are used for identifying the unknown parameters. An objective function is a normalized global error

$$M = \frac{1}{N_s}\sum_{i=1}^{N_s}\left[\left(1-\frac{\bar{F}_i^*}{\hat{\bar{F}}_i^*}\right)^2 + \left(1-\frac{\bar{\delta}_{0i}}{\hat{\bar{\delta}}_{0i}}\right)^2\right] \tag{44}$$

where the hatted values are additional data, such as experimental data, collected from the curves of the force and the depth of the indenters. N_s is the number of sampling data. $\hat{\bar{F}}^*$ and $\hat{\bar{\delta}}_0$ represent the dimensionless values for the force and the depth of the indenter, respectively. $\bar{F}^*$ and $\bar{\delta}_0$ represent those obtained in the inverse analysis, respectively.

These dimensionless variables are defined as

$$\hat{\bar{F}}^* = \frac{\hat{F}}{\mu_n h_1}, \quad \hat{\bar{\delta}}_0 = \frac{\hat{\delta}_0}{h_1} \tag{45}$$

$$\bar{F}^* = \frac{2\pi\bar{a}\bar{p}_0}{\Gamma_n}, \quad \bar{\delta}_0 = \frac{\delta_0}{h_1}. \tag{46}$$

Convergence criteria in the inverse analysis are prescribed as follows:

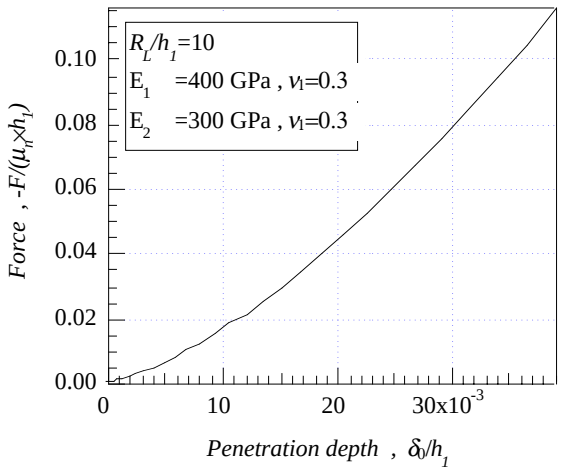

Figure 2 An Example of Penetration Force and Depth

Table 1 Elastic Moduli for Two-Layered Material and Indenter

Region	Young's modulus E_i, GPa	Poisson's ratio ν_i	Ratio of shear moduli $\Gamma_i(=\mu_i/\mu_2)$
Thin film (i=1)	400.00	0.3	2.0
Substrate (i=2)	200.00	0.3	1.0
Indenter (i=3)	1000.00	0.3	5.0

$$M \le 1.0 \times 10^{-5} \ , \quad I_c \le 3000 \tag{47}$$

Where M represents the value of the objective function, and I_c is the count of iteration in the complex method. When either criteria of convergence is satisfied, we considered that the objective function attained to the convergence. Unknown parameters in the complex method were varied within ±30% of true values. The inverse analyses were performed 10 times for various initial values of unknown parameters.

RESULTS OF ANALYSIS

Results for Two-Layered Structures

A contact problem for a layered system which one layer with its thickness of 1μm is coated to a half-region is first analyzed. In this problem, the case where either Young's modulus or Poisson's ratio of film is known is analyzed. Elastic moduli for a two-layered material and for the indenter are shown in Table 1. A curve of the penetration force and the depth of the indenter used in the inverse analysis is shown in Figure 3. Solid circle represents sampling data used in the inverse analysis. Error ratios of identified values to the true values are shown in Figures 4(*a*) and (*b*) for the cases where Young's modulus is known and Poisson's ratio is known, respectively. Figure 4(*b*) shows the errors of identified values for the radius of contact area. The identified Young's modulus is agreed within ±2% with the true values, and the identified Poisson's ratio is within ±4%. This indicates that Young's modulus can be identified easily than Poisson's ratio.

The influence of the number of sampling data on the accuracy of identified values is examined using the paramters employed in the previous analysis. In this analysis, Young's modulus, Poisson's ratio and radii of contact area are all unknown, and the number of sampling points is varied as 3, 6, 9 and 12. Figure 5 shows an example of 12 sampling points. The error ratios of identified elastic moduli to the true values are shown in Figure 6 for the number of data points. It is found that Young's modulus is identified within the error ratio of ±10% using the sampling data more than 5 points, and also the scat-

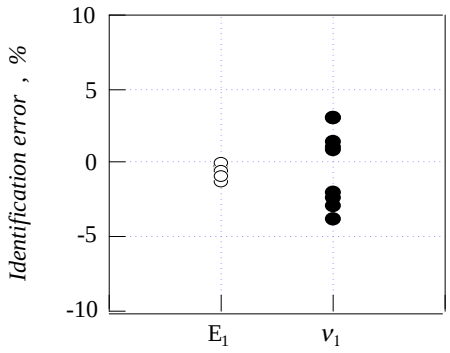

(*a*) Identified Young's Modulus and Poisson's Ratio

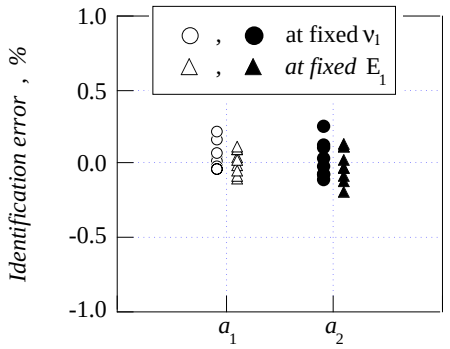

(*b*) Identified Contact Radii

Figure 4 Identification Results for Material with One Layer

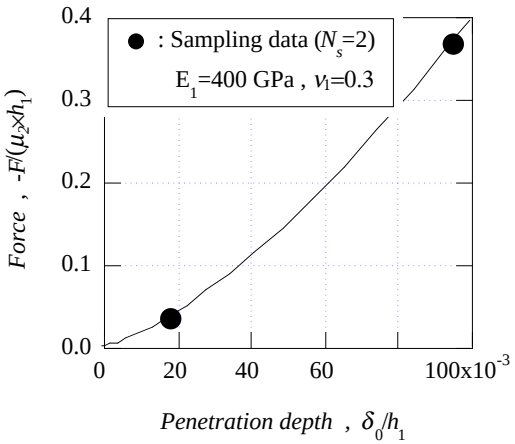

Figure 3 Penetration Force and Depth Curve for R_L/h_1=10

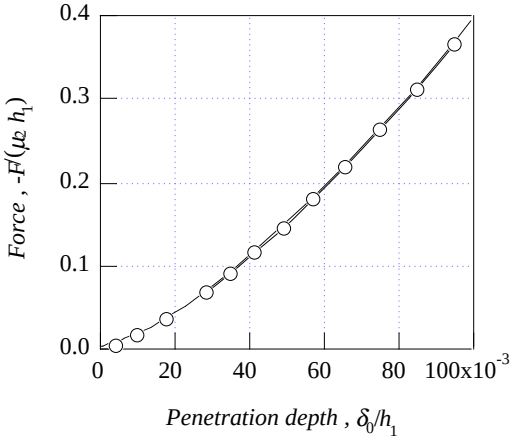

Figure 5 An Example of Sampling Data (N_s=12)

Table 2 Elastic Moduli for Two-Layered Material and Indenter

Region	Young's modulus Ei , GPa	Poisson's ratio ν_i	Ratio of shear moduli $\Gamma_i(=\mu_i/\mu_2)$
Thin film (i=1)	50.00	0.3	0.5
Substrate (i=2)	100.00	0.3	1.0
Indenter (i=3)	1000.00	0.3	10.0

tering of identified Young's modulus tends to decrease. However, even if the number of sampling points increases, the identified Poisson's ratio varies widely. As previously mentioned, it is harder to identify Poisson's ratio than to identify Young's modulus. When the data of sampling points on the force and depth curve for an indenter are used in an identification, we may not be able to expect the increase of the accuracy of identified values. Thus, Young's modulus and Poisson's ratio of a film are determined using simultaneously data on several curves for indenters with various radii of curvature. Material properties used for the inverse analysis are shown in Table 2. Curves of the penetration force and depth for the indenters with radius of curvature of R_L/h_1=10, 20 and 40 are shown in Figure 7 with sampling points. The number of sampling points is 6, and the error ratios of the identified moduli to the true values are shown in Figure 8. The identified values are distributed uniformly around the true values. When this result is compared to the result with data for a single curve, you can see that the deviation and scattering of errors is reduced.

An Identification for Three-Layered Structures In The Case of $E_1>E_2>E_3$

Elastic moduli for a three-layered material are identified strategically using several curves of the force and the depth. A strategic procedure used in this study is described as follows. A parameter with minimum scattering resulted from the first identification analysis is fixed at its average value, and remaining unknown parameters are fixed successively by performing the inverse analysis. Then, the constraint ranges of parameters used in the complex method are set in the variation range of error ratio. This procedure is iterated until the average values of four parameters (E_1, ν_1, E_2, ν_2) are determined. In

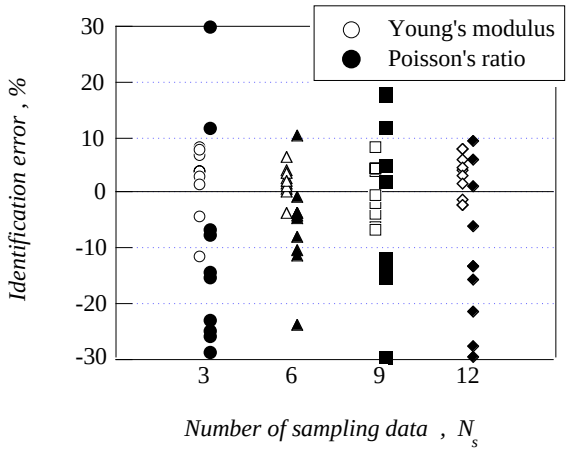

Figure 6 Identification Error for Different Number of Sampling Data

Table 3 Elastic Moduli for Three-Layered Material and Indenter

Region	Young's modulus Ei , GPa	Poisson's ratio ν_i	Ratio of shear moduli $\Gamma_i(=\mu_i/\mu_3)$
Thin film (i=1)	400.00	0.3	2.0
Thin film (i=2)	300.00	0.3	1.5
Substrate (i=3)	200.00	0.3	1.0
Indenter (i=4)	1000.0	0.3	5.0

this analysis, elastic moduli shown in Table 3 are identified. Here, all the films are 1μm in thickness. Sampling points on the curves for three kinds of indenter with the radius of curvature of R_L/h_1=10, 50, 100 are shown in Figure 9. Variation ranges of parameters are set equally for all parameters as the lower limit is 30% of E_2 and the upper limit is 30% of E_1. The error ratios of identified values to the true values are shown in Figures 10(*a*) and (*b*). The variations of error ratios at every each step for identifying four elastic moduli are

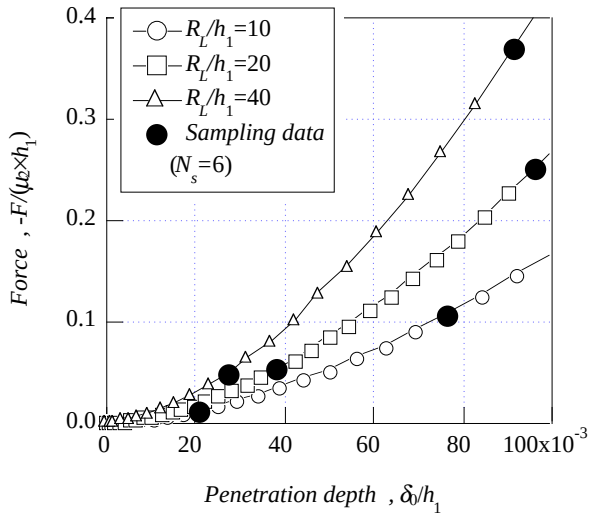

Figure 7 Data Sampling for Identifying Young's Modulus and Poisson's Ratio

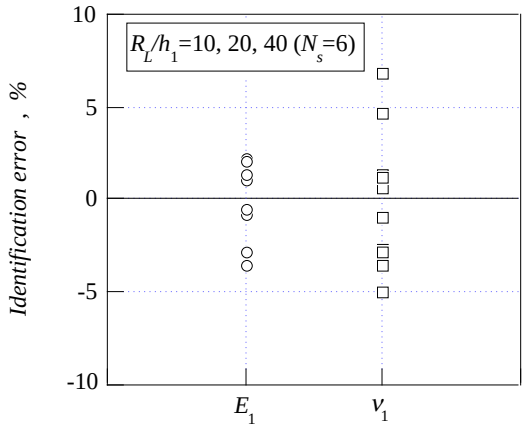

Figure 8 Identified Young's Modulus and Poisson's Ratio

shown in Figure 10(*a*). Figure 10(*b*) represents the error ratios of the identified radii of contact area to the true values. An open circle represents the result of the first step. Since the variation of error for E_1 is minimum within four parameters, E_1 is fixed at 400.8GPa. The identified radii of contact area are very agreed with the true values in a comparison with the identified results of elastic moduli. In this analysis, the radii of contact area are not fixed at a value, and their variation ranges used in the next step are taken as the variation ranges of parameters obtained in the present step. The results of the second step are represented in Figure 10(*a*) by a solid square symbol. Elastic modulus with the minimum scattering of error is Young's modulus for the second layer E_2 and thus E_2 is equated to 302.4GPa of the average of identified values. When the identified values in the first step are compared with those in the second step, the variation of Poisson's ratio fairly reduces. The same procedure is carried out, Poisson's ratio ν_1 for the first layer is fixed at 0.2955 in the third step, and ν_2 for the second layer is fixed at 0.2953 in the forth step. You can see from Figure 10(*b*) that the scattering of identified radii of contact area in the forth step decreases than that in the first step. Final values determined through four steps are listed in Table 4. The identified values, using the same strategic procedure and nine sampling points on a curve of the force and the depth for R_L/h_1=10, are also shown in Table 4. The identified values, using several curves of the force and the depth for the indenters with different radii of curvature, are within errors of ±2%, and those are more accurate than the identified values using nine sampling points on a single curve.

In The Case of $E_1<E_2<E_3$

Next, we try to identify elastic modulii for a three-layered material with a soft layer at the first layer. True values identified in the inverse analysis are shown in Table 5. The procedure for identifying elastic modulii is the same as before. Nine sampling points on three curves for the indenters with three kinds of the radius of curvature (R_L/h_1=10, 20, 40) are shown in Figure 11. The upper and the lower limit of Young's moduli are set to $1.3E_2$ and $0.7E_1$, respectively, and the same constraint ranges of Young's moduli are applied to every layer. The identified results of elastic moduli from the first step to the third step are shown in Figures 12(*a*) and (*b*). It is found that the scattering of error for E_1 is small and E_1 is ease to be identified. However, the average of E_1 is 48.51GPa with the error of –2.98%, and the identified value deviates slightly to a smaller value than the true value. The error ratios of the radii of contact area to the true values are within 1%, however, the scattering of their error ratios is slightly large in comparison with the result shown in Figure 10(*b*). This slight increase of scattering might be cause to a small deviation of Young's modulus of the first layer. The identified values at the second step deviate to larger and smaller values than the true values. This tendency is a feature of identifying the elastic moduli in the three-layered materials with a soft layer at the first layer. When the scattering of the identified values at the second step is examined carefully,

Table 4 Parameters Identified Using Different Data

Parameters	Given value	R_L/h_1= 10,50,100	R_L/h_1=10 (N_s=9)
E_1 [GPa]	400.0	400.8	409.5
ν_1	0.3	0.2955	0.2570
E_2 [GPa]	300.0	302.4	315.6
ν_2	0.3	0.2953	0.2936

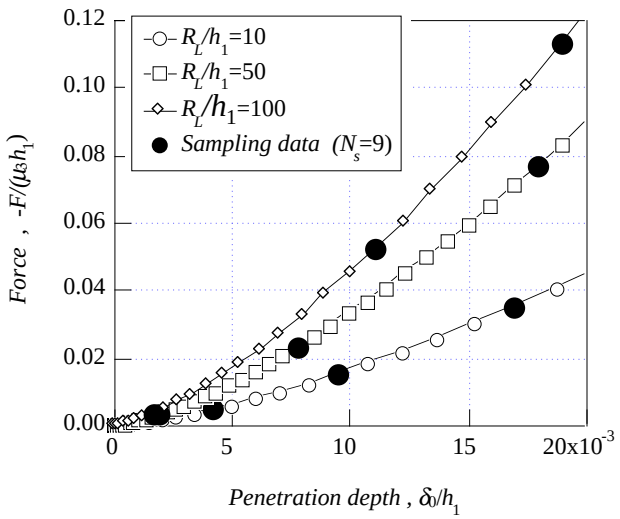

Figure 9 Sampling Data for Inverse Analysis

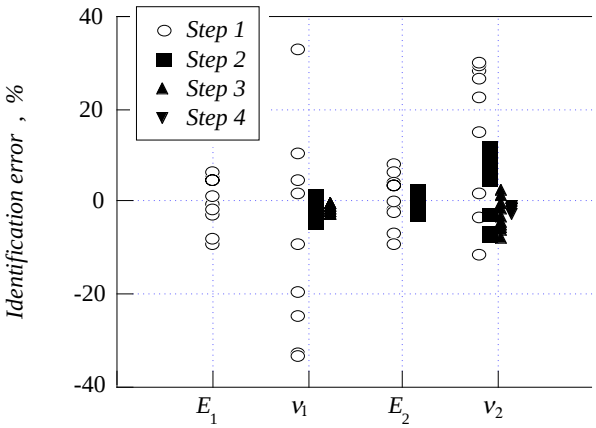

(*a*) Identification Error of Unknown Elastic Moduli

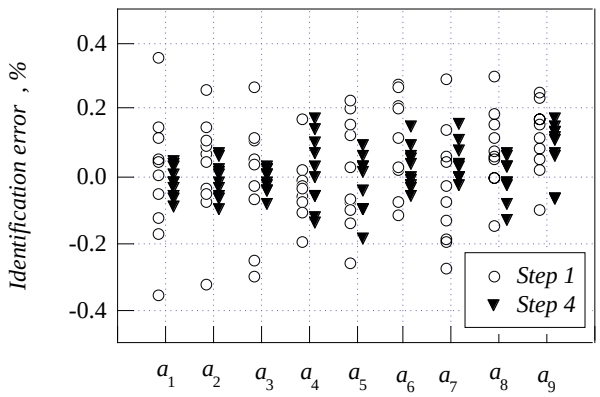

(*b*) Identification Error of Unknown Contact Radii

Figure 10 Identification Error of All Unknown Parameters

Table 5 Elastic Moduli for Three-Layered Material and Indenter

Region	Young's modulus E_i, GPa	Poisson's ratio ν_i	Ratio of shear moduli $\Gamma_i(=\mu_i/\mu_3)$
Thin film (i=1)	50.00	0.3	0.25
Thin film (i=2)	100.00	0.3	0.5
Substrate (i=3)	200.00	0.3	1.0
Indenter (i=4)	1000.0	0.3	5.0

Poisson's ratio for the first layer is fixed at 0.3373 with the error ratio of 12.4%. At the third step, all the identified values are not varied with ten trials for different initial values used in the inverse analysis. Thus, we considered that the objective function attain to a global minimum or a local minimum, and so we stopped to continue the inverse analysis. Final identified values are shown in Table 6. When the identified values for the three-layered material with a hard layer at the first layer are compared to those with a soft layer at the first layer, a new idea is needed for identifying accurately the unknown parameters in the three-layered materials with the soft first layer. We consider that the difficulty for identifying elastic moduli for the three-layered materials is due to the difference of response of the materials in penetrating an indenter. Specifically, comparing the curves of the force and the depth shown in Figure 9 to those shown in Figure 11, the former is more sensitive to the penetration depth than the latter. In the present analysis, additional data are collected from only curves of the force and the depth, so the materials with a high sensitivity for the depth of the indenter have an advantage to approximate the curves using a few data. Thus, when the elastic moduli for the three-layered materials with a soft first layer is identified, we consider that the indenter with a larger radius of curvature should be used for obtaining the curve of the force and the depth.

Identification of The Distribution Function of Elastic Moduli for A Functional Gradient Material

Finally, we suppose that an identification of the distribution function of elastic moduli in a functional gradient material (FGM) is carried out using the indentation data. In this analysis, we consider that Young's modulus and Poisson's ratio are functions of the z-coordinate as follows:

$$E(z) = E_1 \exp(-\alpha z) + E_n\{1-\exp(-\alpha z)\} \tag{48}$$

$$\nu(z) = \nu_1 \exp(-\beta z) + \nu_n\{1-\exp(-\beta z)\} \tag{49}$$

The values of unknown parameters, which should be identified, are shown in Table 7. Where E_n and ν_n are 200GPa and 0.33, which are the values for the substrate, respectively. The variations of elastic moduli are shown in Figure 15. The FGM is 3mm in thickness and is supposed as a four-layered material in the inverse analysis. Assuming one layer to be 1mm in thickness, the same procedure as the pre-

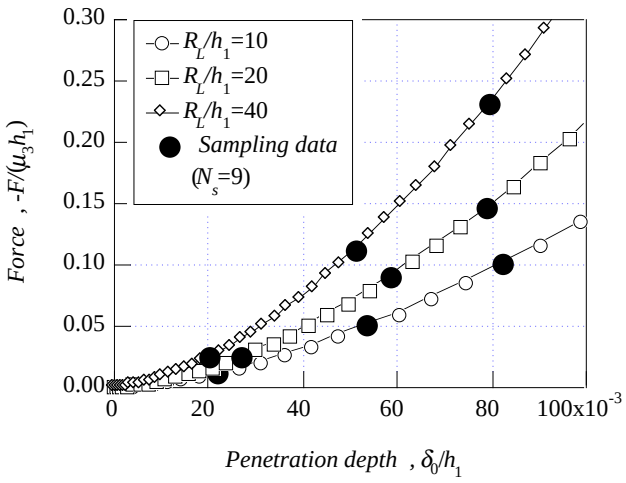

Figure 11 Data Sampling on Penetration Force vs Depth Curve for Three Different Indenters

Table 6 Parameters Identified by Different Data

Parameters	Given value	R_L/h_1= 10,50,100	*error* , %
E_1 [GPa]	50.0	48.51	-2.98
ν_1	0.3	0.3373	12.4
E_2 [GPa]	100.0	93.04	-6.96
ν_2	0.3	0.2733	-8.91

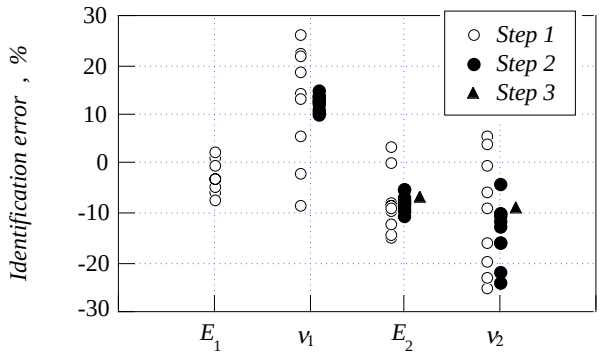

(*a*) Identification Error of Unknown Elastic Moduli

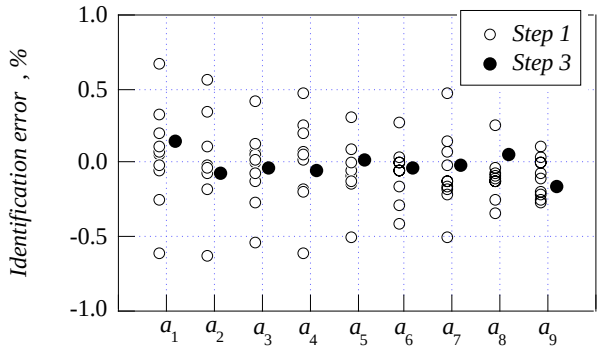

(*b*) Identification Error of Unknown Contact Radii

Figure 12 Identification Error of All Unknown Parameters

Table 7 Identified Parameters of Distribution Function of Elastic Moduli

Parameters	Given values	Identified values	error , %
E_1[GPa]	410.0	395.0	-3.66
ν_1	0.2	0.20596	2.98
α	1000.0	1206.588	20.66
β	600.0	778.9896	29.83

vious inverse analysis is applied to identify the unknown parameters, E_1, ν_1, α and β. Sampling data (nine points) used for the identification are shown in Figure 13. The identified values of parameters are listed in Table 7. Variations of identification errors at every each step are shown in Figure 14. Parameters related with Poisson's ratio is hard to identify accurately, and vary widely. A relationship between the penetration force and depth calculated using the identified values is shown in Figure 13 by dotted lines. It is found that the penetration force and depth using the true values are almost the same as those using the identified values. This means that another information is needed to identify more accurately the distribution functions for elastic moduli. Finally, the variations of elastic moduli estimated using the identified parameters are shown in Figure 15 by thin solid and dotted lines. We consider that the identified parameters can be expressed fairly the variation of elastic moduli.

CONCLUDING REMARKS

In the present paper, a method for identifying elastic moduli for multi-layered materials and for FGM is presented. The method using simulteneously data on several curves of force and depth of the indenters with different radii of curvature is very usefull for identifying the elastic moduli under a limited small number of available data.

REFERENCES

Gladwell,G.M.L., 1980, "Contact Problems in The Classical Theory of Elasticity", Sijthoff & Noordhoff.

Ihara, I., Tokura, K., Aizawa, T., Koguchi, H., Kihara, J., 1994,"Approach for estimating material properties of thin film on substrate by inverse analysis with surface wave spectroscopy Nippon Kikai Gakkai Ronbunshu, Vol.60(579), pp.2664-2671.

Jacoby, S. L. S., Kowalik, J. S., and Pizzo, J. T., 1972, "Iterative Methods for Nonlinear Optimization Problems", Prentice-Hall.

Karasudhi, P. Wijeyewickrema, A C. Lai, T., 1998,"Seismic response to a prescribed seismogram of a body embedded in a multilayered half space", Computational Mechanics, pp.70-76.

Kishimoto,K.,Koeki,Y.,Notomi,M.,Koizumi,T.,1993,"Measurement of elastic modulus of functionally gradient material using inverse analysis", Nippon Kikai Gakkai Ronbunshu, pp.197-202.

Matsui, K. Okada, K., 1997,"Confidence region of estimates from inverse analysis of elastic multilayered system", Advances in Structural Optimization Proceedings of the US-Japan Joint Seminar on Structural Optimization 1997. ASCE, pp.121-132.

Miyamoto, H., 1977, "Theory of Three-Dimensional Elasticity", Shokabo.

Novotny, B., 1992, "Inverse ProblemSolution in Non-Destructive Pavement Diagnostics-Computational Aspects", pp.112-120.

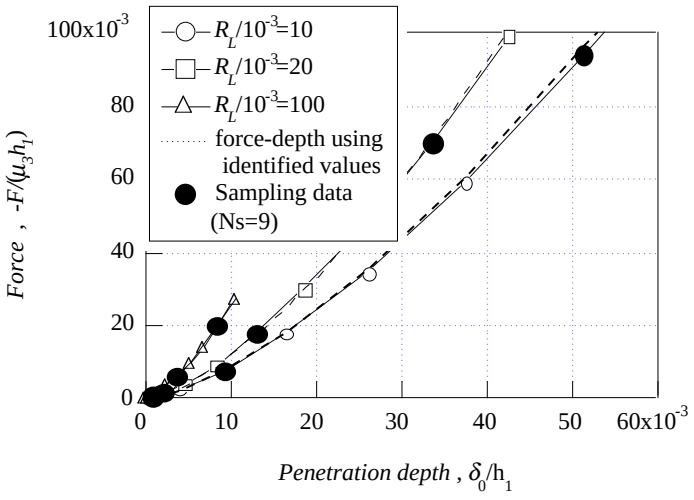

Figure 13 Force-Depth Curve for A FGM and Sampling Data

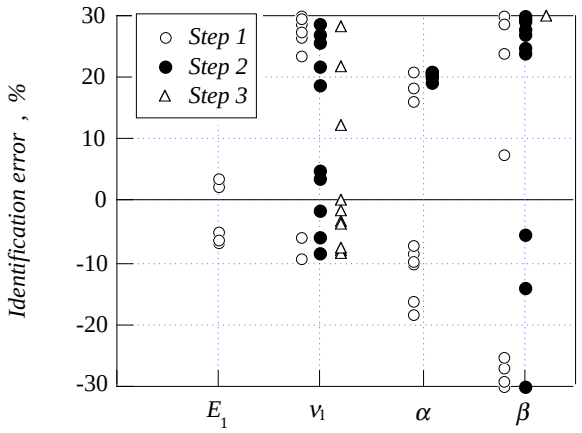

Figure 14 Identification Error Ratios of Parameters

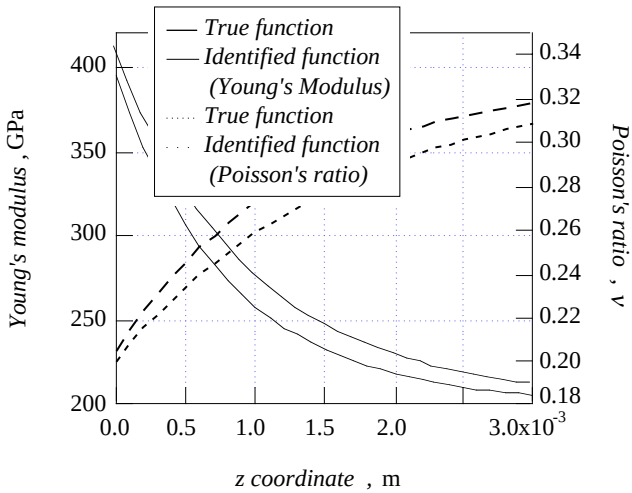

Figure 15 Distribution of Young's Modulus and Poisson's Ratio